Magnetosheath jet properties and evolution as determined by a global hybrid-Vlasov simulation

Minna Palmroth[1,2], Heli Hietala[3], Ferdinand Plaschke[4,5], Martin Archer[6,7], Tomas Karlsson[8], Xóchitl Blanco-Cano[9], David Sibeck[10], Primož Kajdič[9], Urs Ganse[1], Yann Pfau-Kempf[1], Markus Battarbee[1], and Lucile Turc[1]

[1]University of Helsinki, Helsinki, Finland
[2]Finnish Meteorological Institute, Helsinki, Finland
[3]University of California, Los Angeles, USA
[4]Institute of Physics, University of Graz, Graz, Austria.
[5]Space Research Institute, Austrian Academy of Sciences, Graz, Austria.
[6]The Blackett Laboratory, Imperial College London, London, UK
[7]Queen Mary University of London, London, UK
[8]Swedish Institute for Space Physics, Uppsala, Sweden
[9]Instituto de Geofísica, Universidad Nacional Autónoma de México, Mexico City, Mexico
[10]Code 674, NASA/GSFC, Greenbelt, MD, USA

Correspondence to: Minna Palmroth (minna.palmroth@helsinki.fi)

Abstract. We use a global hybrid-Vlasov simulation for the magnetosphere, Vlasiator, to investigate magnetosheath high-speed jets. Unlike many other hybrid-kinetic simulations, Vlasiator includes an unscaled geomagnetic dipole, indicating that the simulation spatial and temporal dimensions can be given without scaling. Thus, for the first time, this allows investigating the magnetosheath jet properties and comparing them directly with the observed jets within the Earth's magnetosheath. In

5   the run shown in this paper, the interplanetary magnetic field (IMF) cone angle is $30°$, and a foreshock develops upstream of the quasi-parallel magnetosheath. We visually detect a structure with high dynamic pressure propagating from the bow shock towards the magnetopause. The structure is confirmed as a jet using three different criteria, which have been adopted in previous observational studies. We compare these criteria against the simulation results. We find that the magnetosheath jet is an elongated structure extending Earthward of the bow shock by $\sim$2.3 R_E, while its size perpendicular to the direction

10   of propagation is $\sim$0.5 R_E. We also investigate the jet evolution, and find that the jet originates due to the interaction of the foreshock Ultra Low Frequency (ULF) waves with the bow shock surface. The simulation shows that magnetosheath jets can develop also under steady IMF, as inferred by observational studies.

1   Introduction

Solar wind plasma encompasses the Earth's magnetic domain with a region of turbulent magnetosheath, consisting of shocked

15   plasma. The sunward boundary of this region is the bow shock through which the plasma flows into the magnetosheath. The earthward boundary of the magnetosheath is the magnetopause, the outer edge of Earth's magnetic domain. The bow shock and magnetosheath plasma properties relative to those in the upstream pristine solar wind depend broadly on the interplanetary

magnetic field (IMF) direction. One of the most important parameters is the bow shock normal direction. In portions of the bow shock, where the bow shock normal is more or less parallel to the IMF direction, the bow shock is said to be *quasi-parallel*. At the quasi-parallel shock, part of the solar wind particles reflect back towards the Sun (Schwartz et al., 1983; Meziane et al., 2004), causing instabilities and waves upstream, and forming a so-called foreshock. The downstream part of the quasi-parallel

5   shock is called the quasi-parallel magnetosheath, where the plasma properties are highly turbulent (e.g., Fuselier et al. 1991; Gutynska et al. 2012). On the other hand, the quasi-perpendicular side of the bow shock is less turbulent, and there is no foreshock upstream because the reflected particles keep close to the bow shock and the waves do not have time to grow. The magnetosheath downstream of the quasi-perpendicular bow shock hosts a variety of waves, e.g., mirror mode waves (Soucek et al., 2015; Hoilijoki et al., 2016).

10   Němeček et al. (1998) reported observations of peaks in the ion fluxes within the quasi-parallel magnetosheath, which they termed transient flux enhancements. Hietala et al. (2009) reported observations of similar high velocities near the magnetopause, and proposed a mechanism to produce these velocities by a rippled bow shock surface. In this mechanism the distorted bow shock surface collimates particles into a structure termed a magnetosheath jet. Several studies have investigated the properties of these jets and demonstrated their importance in terms of geoefficiency, as they can for example distort the

15   magnetopause (Shue et al., 2009; Plaschke et al., 2016). Jets are also important for magnetospheric dynamics because they can trigger magnetopause reconnection (Hietala et al., 2018). Statistical investigations of the jets show that they are clearly associated with the foreshock and the quasi-parallel magnetosheath (e.g., Archer and Horbury 2013; Plaschke et al. 2013). Omidi et al. (2016) therefore suggested that foreshock waves may be related to the origin of the jets.

The jets have later been identified using a variety of measurement criteria. Since the jets exhibit high velocities and/or

20   densities, Plaschke et al. (2013) devised a criterion C_P, defined as the ratio of the magnetosheath dynamic pressure in the X direction and the upstream solar wind dynamic pressure. Plaschke et al. (2013) defined that in order to represent jets, C_P had to fulfil the condition

$$C_P = \frac{\rho v_X^2}{\rho_{sw} v_{sw}^2} > 0.25, \tag{1}$$

where ρ is the density, v_X is the velocity component in the X direction, the numerator refers to the conditions in the magne-

25   tosheath while the denominator represents solar wind conditions, with the subscript sw denoting the solar wind. The coordinate system that they used was Geocentric Solar Ecliptic (GSE), where X is sunward, Z is perpendicular to the ecliptic plane and is positive northward, and Y completes the righthanded system. The Plaschke criterion C_P defines the jet as the entire region where Eq. (1) holds, and requires that the dynamic pressure peak is >0.5 times the solar wind value. Further, the criterion is applied only for solar zenith angles less than $30°$.

30   Archer and Horbury (2013) used the total dynamic pressure but divided by a 20-minute temporal average of the dynamic pressure within the surrounding magnetosheath, and required that

$$C_A = \frac{\rho v^2}{< \rho_{sh} v_{sh}^2 >_{20min}} > 2. \tag{2}$$

Karlsson et al. (2012) investigated enhancements in the magnetosheath density, which they called plasmoids. They separated the plasmoids according to their speed, and observed that the fast plasmoids have 10% increase in local velocity, and that therefore they could be associated with jets. They defined the events by taking ratios of the magnetosheath electron density to a 15-minute temporal average within the magnetosheath as

$$C_K = \frac{n_e}{<n_e>_{15min}} > 1.5, \tag{3}$$

where n_e is the electron density in the magnetosheath. Both C_A and C_K are only defined to identify peak values of the relevant parameters, and when durations or spatial scales were identified the full-width-at-half-maximum was used. Jets identified with the three criteria are in broad agreement with respect to occurrence and properties, suggesting that the criteria identify similar phenomena. This motivates a modelling study to test how similar the three criteria in fact are and whether they all are associated with magnetosheath jets.

Hao et al. (2016) performed local hybrid-particle-in-cell (PIC) simulations within a limited spatial extent, and found that the solar wind Alfvén Mach number is important in determining how far the jets can penetrate within the magnetosheath. Using a 2D hybrid-PIC code, Karimabadi et al. (2014) observed jet-like structures penetrating from the foreshock to the magnetosheath. The structures were elongated regions of higher magnetic field and plasma density. However, since Karimabadi et al. (2014) use a scaled dipole strength in the hybrid-PIC model, representative of roughly a Mercury-sized magnetosphere, deducing the scale sizes of the structures from the simulation results is not straightforward, and their direct comparison to the jets observed in the Earth's magnetosheath is difficult. Nevertheless, Karimabadi et al. (2014) reported that jet scales parallel to the direction of propagation could be $\sim$2.4 R_E, and in the perpendicular direction $\sim$0.3 R_E within the Earth's magnetosheath. Plaschke et al. (2016) estimate observationally that the jet sizes are 1.34 R_E by 0.71 R_E in the parallel and perpendicular direction, respectively.

In this paper, we use the hybrid-Vlasov simulation code Vlasiator to investigate the jet properties. Vlasiator includes ion-kinetic features similar to hybrid-PIC codes, but unlike hybrid-PIC codes, does not include sampling noise in the results due to a different modelling approach. Further, Vlasiator uses the actual unscaled geomagnetic dipole strength as a boundary condition, and therefore the results can be given in R_E and seconds without scaling, indicating that the length and time scales can be directly compared to spacecraft observations of jets. In this paper, we first introduce Vlasiator, and the run used to examine the magnetosheath jets. We visually identify a candidate jet, after which we show that our candidate jet fulfils all three jet criteria described above. We then examine the jet properties and evolution, and end the paper with discussion and conclusions.

2 Model

Vlasiator is a hybrid-Vlasov model targeted for global simulations of the Earth's magnetosphere. Vlasiator solvers treat protons as a distribution function $f(\mathbf{r}, \mathbf{v}, t)$ in phase space, and electrons as a charge-neutralizing fluid (Palmroth et al., 2013; von Alfthan et al., 2014; Palmroth et al., 2015; Pfau-Kempf, 2016). Electron kinetic effects are neglected by the solvers, but

the ion kinetic effects are solved without numerical noise. The time-evolution of $f(\mathbf{r}, \mathbf{v}, t)$ is controlled by the Vlasov equation, propagated by a fifth-order accurate semi-Lagrangian approach (Zerroukat and Allen, 2012; White and Adcroft, 2008). Maxwell's equations neglecting the displacement current in the Ampère-Maxwell law are used to solve the electromagnetic fields. Maxwell's equations are supplemented by Ohm's law, including the Hall term. The technical features of the code including the closure scheme, the numerical approach, and the parallelization techniques are described by von Alfthan et al. (2014) in the previous version using the Finite Volume Method, while here and in Palmroth et al. (2015) an updated Semi-Lagrangian scheme is used (see also Pfau-Kempf 2016).

The run investigated in this paper is carried out in the ecliptic XY plane of the Geocentric Solar Ecliptic (GSE) coordinate system, representing a two-dimensional (2D) approach in ordinary space. Each ordinary space simulation cell includes a 3D velocity space used to describe the proton velocity distribution. Therefore the approach here is 5D in total. The simulation plane in the run used in this paper ranges from $-7.9\ R_E$ to $46.8\ R_E$ in X, and $\pm 31.3\ R_E$ in Y, with a resolution of 228 km corresponding to the typical ion inertial length in the solar wind. The velocity space resolution is 30 km/s. The solar wind parameters are given as an input at the sunward wall of the simulation box, while copy conditions are applied at other boundaries. The Z direction in ordinary space applies periodic conditions. The inner edge of the magnetospheric domain is a circle with a radius of 5 R_E, while the ionosphere is a perfect conductor in the present version of the code.

The solar wind parameters in this run are as follows: The IMF has a cone angle of 30°, the IMF x component is -4.33 nT, IMF y is 2.5 nT, while the total magnetic field intensity is 5 nT. The solar wind density is 1 cm^{-3}, and velocity 750 kms^{-1} in the $-X$ direction. Solar wind distribution functions are assumed Maxwellian, with an initial temperature of 0.5 MK. This same run has previously been used to investigate magnetosheath mirror mode waves by Hoilijoki et al. (2016).

3 Results

Figure 1a shows a close-up of the Vlasiator simulation domain investigated in this paper. It shows a snapshot of a supplementary movie S1, depicting the dynamic pressure at time $t = 305.5$ s from the beginning of the run. Colour-coding shows the dynamic pressure. Based on movie S1, we visually identified a high-pressure structure emerging from the bow shock surface and extending through the magnetosheath, marked with a white arrow. The white dot in Fig. 1a shows the earthward edge of this structure, from which we show virtual spacecraft data in Fig. 1b. The virtual spacecraft data in Fig. 1b shows that the velocity increased roughly by 20%, density roughly by 50%, while the dynamic pressure roughly doubled at the time of the structure in panel 1a, marked by a vertical dashed line.

Figure 2 shows the Plaschke criterion C_P defined in Eq. (1), where colour-coding shows the dynamic pressure ratio between the magnetosheath and solar wind, using the X component of the velocity v_X. The black contour shows where this quantity exceeds 0.25, while the white contour shows the area where the quantity exceeds 0.5 in line with Plaschke et al. (2013). The structure in Fig. 1 can be observed as an elongated feature starting from the bow shock and extending to the left towards the magnetopause in Fig. 2 approximately at $X, Y = [10, -4]R_E$.

Figure 3 shows the Archer and Horbury criterion C_A (Eq. 2), which is a ratio of the dynamic pressure and the temporal average of dynamic pressure. Panel 3a shows this ratio, panel 3b is the dynamic pressure (the numerator of the criterion), and panel 3c shows the temporal average of dynamic pressure (the denominator of the criterion). While Archer and Horbury (2013) originally used a 20-minute average in the denominator, here we use a three-minute temporal average, centered on time

5    $t = 305.5$ s. This is solely because the simulation interval does not last for 20 minutes, and while testing different values this three-minute average was found to be the shortest period identifying the structure, while having a manageable amount of data. The contours in panel 3a show where the Archer and Horbury criterion exceeds 2, and where therefore the dynamic pressure is twice the temporal average. The largest area satisfying this criterion can be found near the location $X, Y = [10, -4]R_E$.

Figure 4 shows the Karlsson criterion C_K (Eq. 3), namely the ratio of the instantaneous density to the temporal average of

10   the density. Panel 4a shows this ratio. Panels 4b and 4c show the density and the temporal average of density over three minutes, centered on the time $t = 305.5$ s, respectively. The contour in panel 4a shows locations where the ratio exceeds 1.5., that is where the density is 50% greater than the temporal average. Figure 4a shows that the Karlsson criterion is fulfilled mostly at the surface of the bow shock, while a small area of higher density can be found at location $X, Y = [9, -4]R_E$.

Finally, Fig. 5 compares results for all the criteria, the Karlsson criterion C_K in Eq. (3) with magenta, Archer and Horbury

15   criterion C_A in Eq. (2) with blue, and the Plaschke criterion in Eq. (1) with a black contour. The region we visually identified from the movie S1, and which is indicated by an arrow in Fig. 1a fulfils all three criteria approximately at $X, Y = [10, -4]R_E$. Since the criteria agree, we call the feature a magnetosheath jet, and identify its physical dimensions and evolution in time. We adopt an inclusive strategy, and determine that the jet originates at the bow shock with enhanced C_K (magenta) criterion, at $X = 11.6\ R_E$, and reaches a location with enhanced C_A (blue) criterion at $X = 9.1\ R_E$. Taking into account the angle at

20   which the magnetosheath jet propagates from the bow shock towards the magnetopause, its length is approximately 2.3 R_E in the direction of propagation. In the perpendicular direction, the jet size varies from 0.6 R_E at the bow shock, to 0.3 R_E in the mid-jet area, to ~0.5 R_E at the magnetopause end. Since Fig. 5 represents a snapshot, we emphasise that these dimensions are instantaneous values.

Next we examine the jet evolution in time, using the Plaschke criterion. Figures 6a-d show the total dynamic pressure in the

25   background, and the Plaschke criterion as a cyan contour at four times near the time shown in Fig. 5. The panels are snapshots from Supplementary movie S2. In Fig. 6a, a high-pressure area shown by the white arrow approaches the bow shock. This area, which is associated with 30-second ULF waves in the foreshock (Palmroth et al., 2015), steepens towards the bow shock surface. At time $t = 295$ s the higher dynamic pressure area has hit the bow shock, shown by the arrow in Fig. 6b. In panels 6c and 6d this bulge extends towards the magnetopause, and at time $t = 310$ s it is already fading away. Supplementary movie

30   S2 shows this time sequence in a more dynamic fashion. Figure 6 shows that the jet is at its prime at the time shown in Fig. 5, indicating that the jet dimensions given above are to be taken as maximum values at least for driving parameters similar to the ones in this run.

4 Discussion

In this paper, we have presented a Vlasiator simulation run in the ecliptic plane with a 30° IMF cone angle. We identify and study a magnetosheath jet, and verify its properties by comparing to three observational criteria (Plaschke et al., 2013; Archer and Horbury, 2013; Karlsson et al., 2012, 2015). The fact that the structure we observed fulfilled all three observational

5   criteria indicates that the observations of Plaschke et al. (2013); Archer and Horbury (2013); Karlsson et al. (2015) indeed concern similar phenomena within the magnetosheath. The fact most supporting the idea that our visually selected event is indeed a magnetosheath jet is that all three criteria agree spatially within the jet, and that the identified region is continuous starting from the shock surface and reaching towards the magnetopause. Further, it has a limited lifetime during which the criteria are met within the same region, suggesting that the origin has to do with temporal changes that are connected by the

10   three criteria. While we have concentrated on one jet, there are many more candidate jets in this Vlasiator run that satisfy the different criteria, as shown by the Supplementary movies S1 and S2. This and other runs carried out with Vlasiator will allow investigations looking into the evolution of the jets as a function of their position inside the magnetosheath, and how this depends on the driving conditions.

    We find that the jet size in the direction of propagation is 2.3 R_E, while in the perpendicular direction it is ∼0.5 R_E in size.

15   These dimensions are in agreement with previous scaled results given in ion inertial lengths within a hybrid-PIC simulation with roughly a Mercury-size magnetic dipole, assuming typical magnetosheath properties in order to convert the results into Earth radii (Karimabadi et al., 2014). Plaschke et al. (2016) estimate the size of the jets to be 1.34 R_E by 0.71 R_E. The difference to our results may be because we selected the most prominently visible jet, which reached deepest into the magnetosheath, and we measured the dimensions at the prime of the jet. In the simulation, the entire jet can be measured and the flow parallel

20   direction can be identified. Spacecraft instead will rarely cross the jet along that axis of largest extension. Thus the jet in our results may be more elongated than the ones in Plaschke et al. (2016), although the Supplementary movies S1 and S2 indicate many other smaller jet-like structures with dimensions better in accordance with observations.

    It is interesting to compare the different observational criteria in Eqs. (1-3) in light of the simulation results shown here. According to Plaschke et al. (2018), the Archer and Horbury criterion is most inclusive, identifying a large amount of jets,

25   while the Karlsson criterion is most strict identifying small amounts of jets (or plasmoids). We have not rigorously tested how large areas the three criteria in fact concern within the magnetosheath, as we have concentrated in finding a structure that could be identified as a jet with the present observational criteria. We note however that based on Fig. 5 both the Archer and Horbury (2013) and the Plaschke et al. (2013) criteria identify larger regions than the Karlsson criterion, which indeed seems to be the most strict in the simulation overall.

30   We find that the Karlsson criterion is mostly enhanced near the bow shock surface, and it seldom reaches the magnetosheath portions close to the magnetopause. On the contrary, the Archer and Horbury (2013) criterion identifies regions closest to the magnetopause but can be found to be satisfied throughout the magnetosheath, agreeing with the observational statistics. These characteristics might be associated with the solar wind driving conditions in our run. Neither Karlsson et al. (2012) nor Karlsson et al. (2015) specify the solar wind conditions for their events, while our event is associated with the solar wind density value

of 1 cm^{-3}. The Archer and Horbury criterion is determined by the dynamic pressure depending quadratically on the velocity, which in our simulation is rather high in the solar wind, 750 kms^{-1}. While both criteria concern ratios that can be enhanced during a variety of driving conditions, it is possible that in the conditions of this run, the Karlsson high-density plasmoids are either not properly generated or cannot propagate deep in the magnetosheath, while the Archer and Horbury pressure

5   enhancements could traverse further towards the magnetopause due to the faster general velocities in the magnetosheath. In accordance with Plaschke et al. (2013), the Plaschke criterion in our results is most enhanced near the bow shock. This may be because it is based on the X component of dynamic pressure: The general magnetosheath flow pattern starts to deviate from the X direction rather soon after the shock. Further, the jets push ambient magnetosheath plasma out of their way in order to reach the magnetopause, decelerating them to a level where they no longer satify the Plaschke criterion. Therefore, in order to

10   observe more jets close to the magnetopause, it may be better to choose the Archer and Horbury (2013) criterion.

By looking at the Supplementary movie S2 and Fig. 6, we find that the jet in question is formed by the interaction of a steepened foreshock ULF wave with the bow shock surface. These ULF waves are common in the foreshock, where they advect towards the bow shock near which they are steepened, acquiring a high dynamic pressure (e.g. Eastwood et al., 2005, and references therein). The ULF pressure fluctuations within the foreshock convecting towards the bow shock arrive there

15   with a variety of properties. The foreshock pressure enhancement associated with the selected jet has a larger pressure than its neighbours. It is also elongated along the X axis, and wider in Y than other foreshock fluctuations within the run sequence. Further, the bow shock already shows an initial dent before the pressure front arrives there. Therefore, the pressure enhancement passes the bow shock with little braking and can propagate deep into the magnetosheath. In contrast, we refer to another larger pressure fluctuation reaches the bow shock at about $t = 351$ s (at $X, Y \approx [11, -3.5]R_E$, see movie S2). The bow shock is not

20   dented upon the arrival of this fluctuation and therefore the resulting jet-like structure does not grow large or propagate very deep within the magnetosheath. Since there is only one larger jet in this run sequence, we cannot yet say how common this ULF wave interaction is, but shall certainly come back to the connection in future runs.

Both Omidi et al. (2016) and Hao et al. (2016), using a 2D hybrid-PIC simulation, associate magnetosheath jet-like structures to foreshock ULF waves. The jets in Omidi et al. (2016) are also associated with high dynamic pressures, and they reach close

25   towards the magnetopause. They note that "these regions are not associated with high flow speeds and are instead caused by the density enhancements associated with the magnetosheath filamentary structures". Without a rigorous comparison to the data in Omidi et al. (2016) we cannot be sure that the features in their simulation and the ones shown here concern the same physics and whether therefore the origins of the structures can be related. However, we do note that in our simulations the higher dynamic pressure regions within the magnetosheath, which we call the magnetosheath jets, are associated with high

30   velocities.

For the generation of the jets, Hietala et al. (2009) suggested a mechanism, which relies on an assumption of a rippled shock surface that actively funnels particles into a collimated structure having a high velocity, propagating towards the magnetopause. Hietala et al. (2009) discussed the origins of such a ripple and remarked that while rippling is inherent to the quasi-parallel shock, one possible origin for the ripple would be a short, large-amplitude magnetic structure (SLAMS) (e.g. Lucek et al., 2002)

35   convecting towards the bow shock and interacting with it. Further, Karlsson et al. (2015) suggested that SLAMS interaction

with the bow shock could lead to the formation of their plasmoid observations. The jet we have investigated here is directly associated with a high-pressure foreshock structure interacting with the bow shock. While we do not take a position whether our high-pressure structure causing the jet is indeed a SLAMS, we note that our result presents evidence that the origin of the ripple may be caused by an interaction of the bow shock with the foreshock. As the foreshock ULF wave interaction with the

5   bow shock has also been suggested to provide seed perturbations for the mirror mode waves within the quasi-perpendicular magnetosheath (Hoilijoki et al., 2016), we note that it is becoming vital to understand the foreshock processes as a driver for many kinetic phenomena within the magnetosheath.

5   Conclusions

We investigated magnetosheath high-speed jets in a hybrid -Vlasov simulation done at scales directly comparable to the Earth's

10 magnetosphere. We identify structures in the simulation that can be related to the magnetosheath jets using three different observational criteria. We examine one such jet in more detail and find that its maximum size is 2.3 R_E and $\sim$0.5 R_E in the direction parallel and perpendicular to the propagation direction, respectively. The jet originates from the interaction of the foreshock ULF waves with the bow shock.

Acknowledgements. We acknowledge The European Research Council for Starting grant 200141-QuESpace, with which Vlasiator (http:

15 //physics.helsinki.fi/vlasiator) was developed, and Consolidator grant 682068-PRESTISSIMO awarded to further develop Vlasiator and use it for scientific investigations. We gratefully also acknowledge the Finnish Centre of Excellence in Research of Sustainable Space (Academy of Finland grant number 312351), Academy of Finland grant numbers 267144, and 309937. PK's work was supported by DGAPA/PAPIIT grant IA104416. The CSC − IT Center for Science in Finland is acknowledged for the Grand Challenge award leading to the results shown in here. We acknowledge valuable discussions within the International Space Science Institute (ISSI) team 350, called "Jets downstream of

20 collisionless shocks", led by FP and HH. LT acknowledges Marie Sklodowska-Curie grant 704681.

References

von Alfthan, S., Pokhotelov, D., Kempf, Y. ., Hoilijoki, S., Honkonen, I., Sandroos, A. and Palmroth, M.: Vlasiator: First global hybrid-Vlasov simulations of Earth's foreshock and magnetosheath, *J. Atmos. Solar Terr. Phys.*, 120, 24-35, doi:10.1016/j.jastp.2014.08.012, 2014.

5   Archer, M. O., and Horbury, T. S.: Magnetosheath dynamic pressure enhancements: occurrence and typical properties, Ann. Geophys. 31, 319-331, doi:10.5194/angeo-31-319- 2013, 2013

Eastwood, J. P., Balogh, A., Lucek, E. A., Mazelle, C., and Dandouras, I., Quasi-monochromatic ULF foreshock waves as observed by the four-spacecraft Cluster mission: 1. Statistical properties, J. Geophys. Res., 110, A11219, doi:10.1029/2004JA010617, 2005

Fuselier, S., Klumpar, D., and Shelley, E.: On the origins of energetic ions in the Earth's dayside magnetosheath, J. Geophys. Res., 96, 47-56, 10   1991.

Gutynska, O., Šimunek, J., Šafránková, J., N?meček, Z., and Přech, V.: Multipoint study of magnetosheath magnetic field fluctuations and their relation to the foreshock, J. Geophys. Res., 117, A04214, doi:10.1029/2011JA017240, 2012

Hao, Y., Lembege, B., Lu, Q., and Guo, F., Formation of downstream high-speed jets by a rippled nonstationary quasi-parallel shock: 2-D hybrid simulations, J. Geophys. Res., 121, 2080-2094, doi:10.1002/2015JA021419, 2016

15   Hietala, H., Laitinen, T. V., Andréeová, K., Vainio, R., Vaivads, A., Palmroth, M., Pulkkinen, T. I., Koskinen, H. E. J., Lucek, E. A., Rème, H.: Supermagnetosonic Jets behind a Collisionless Quasiparallel Shock, Phys. Rev. Lett. 103(24), 245001, doi:10.1103/PhysRevLett.103.245001, 2009

Hietala, H., Phan, T.D., Angelopoulos, V., Oieroset, M., Archer, M. O., Karlsson, T., and Plaschke, F.: In situ observations of a magnetosheath high-speed jet triggering magnetopause reconnection, Geophys. Res. Lett., 45, doi:10.1002/2017GL076525, 2018

20   Hoilijoki, S., Palmroth, M., Walsh, B. M., Pfau-Kempf, Y., von Alfthan, S., Ganse, U., Hannuksela, O. and Vainio, R.: Mirror modes in the Earth's magnetosheath: Results from a global hybrid-Vlasov simulation, *J. Geophys. Res. Space Physics*, 121, doi:10.1002/2015JA022026, 2016.

Karimabadi, H., Roytershteyn, V., Vu, H. X., Omelchenko, Y. A., Scudder, J., Daughton, W., Dimmock, A., Nykyri, K., Wan, M., Sibeck, D. G., Tatineni, M., Majumdar, A., Loring, B., and Geveci, B.: The link between shocks, turbulence, and magnetic reconnection in 25   collisionless plasmas, Phys. of Plasmas, 21, 062308, doi: 10.1063/1.4882875, 2014

Karlsson, T., Brenning, N., Nilsson, H., Trotignon, J.-G., Vallières, X., and Facsko, G.: Localized density enhancements in the magnetosheath: Three-dimensional morphology and possible importance for impulsive penetration, J. Geophys. Res. 117, 03227, doi:10.1029/2011JA017059, 2012

Karlsson, T., Kullen, A., Liljeblad, E., Brenning, N., Nilsson, H., Gunell, H., and Hamrin, M.: On the origin of magnetosheath plasmoids 30   and their relation to magnetosheath jets, J. Geophys. Res. 120, 7390-7403, doi:10.1002/2015JA021487, 2015

Lucek, E. A., Horbury, T. S., Dunlop, M. W., Cargill, P. J., Schwartz, S. J., Balogh, A., Brown, P., Carr, C., Fornacon, K.-H., and Georgescu, E.: Cluster magnetic field observations at a quasi-parallel bow shock, Ann. Geophys., 20, 1699-1710, https://doi.org/10.5194/angeo-20-1699-2002, 2002.

Meziane, K., Mazelle, C., Wilber, M., LeQuéau, D., Eastwood, J. P., Rème, H., Dandouras, I., Sauvaud, J. A., Bosqued, J. M., Parks, 35   G. K., Kistler, L. M., McCarthy, M., Klecker, B., Korth, A., Bavassano-Cattaneo, M.-B., Lundin, R., and Balogh, A.: Bow shock specularly reflected ions in the presence of low-frequency electromagnetic waves: a case study, Ann. Geophys., 22, 2325-2335, https://doi.org/10.5194/angeo-22-2325-2004, 2004.

Němeček, Z., Săfránková, J., Přech, L., Sibeck, D. G., Kokubun, S., Mukai, T.: Transient flux enhancements in the magnetosheath, Geophys. Res. Lett. 25, 1273-1276, doi:10.1029/98GL50873, 1998

Omidi, N., Berchem, J., Sibeck, D., and Zhang, H.: Impacts of spontaneous hot flow anomalies on the magnetosheath and magnetopause, J. Geophys. Res. Space Physics, 121, 3155-3169, doi:10.1002/2015JA022170, 2016.

5 Palmroth, M., Honkonen, I., Sandroos, A., Kempf, Y., von Alfthan, S. and Pokhotelov, D.: Preliminary testing of global hybrid-Vlasov simulation: Magnetosheath and cusps under northward interplanetary magnetic field, *J. Atmos. Solar Terr. Phys.*, 99, 41-46, doi:10.1016/j.jastp.2012.09.013, 2013.

Palmroth, M., Archer, O., Vainio, R., Hietala, H., Pfau-Kempf, Y., Hoilijoki, S., Hannuksela, O., Ganse, U., Sandroos, A., von Alfthan, S. and Eastwood, J.: ULF foreshock under radial IMF: THEMIS observations and global kinetic simulation Vlasiator results compared, J.

10   Geophys. Res., doi:10.1002/2015JA021526, 2015.

Pfau-Kempf, Y., Vlasiator: From local to global magnetospheric hybrid-Vlasov simulations, Doctoral thesis, University of Helsinki, URN:ISBN:978-952-336-001-3, http://urn.fi/URN:ISBN:978-952-336-001-3, 2016

Plaschke, F., Hietala, H., Angelopoulos, V.: Anti-sunward high-speed jets in the subsolar magnetosheath, Ann. Geophys. 31, 1877-1889, doi:10.5194/angeo-31-1877-2013, 2013

15 Plaschke, F., Hietala, H., Angelopoulos, V., and Nakamura, R.,: Geoeffective jets impacting the magnetopause are very common, J. Geophys. Res. Space Physics, 121, 3240-3253, doi:10.1002/2016JA022534, 2016

Plaschke, F., Hietala, H., Archer, M., Blanco-Cano, X., Kajdič, P., Karlsson, T., Lee, S.-H., Omidi, N., Palmroth, M., Roytershteyn, V., Schmid, D., Sergeev, V., and Sibeck, D., Jets downstream of collisionless shocks, submitted to Space Sci. Rev., 2018

Schwartz, S. J., Thomsen, M. F., and Gosling, J. T., Ions upstream of the Earth's bow shock: A theoretical comparison of alternative source

20   populations, J. Geophys. Res., 88(A3), 2039-2047, doi:10.1029/JA088iA03p02039, 1983

Shue, J.-H., Chao, J.-K., Song, P., McFadden, J. P., Suvorova, A., Angelopoulos, V., Glassmeier, K. H., and Plaschke, F.,: Anomalous magnetosheath flows and distorted subsolar magnetopause for radial interplanetary magnetic fields, Geophys. Res. Lett., 36, L18112, doi:10.1029/2009GL039842, 2009.

Soucek, J., Escoubet, C. P., and Grison, B.,: Magnetosheath plasma stability and ULF wave occurrence as a function of location in the

25   magnetosheath and upstream bow shock parameters, J. Geophys. Res. Space Physics, 120, 2838-2850, doi:10.1002/2015JA021087, 2015.

White, L. and Adcroft, A.: A high-order finite volume remapping scheme for nonuniform grids: The piecewise quartic method (PQM), J. Comp. Phys., 227, 7394-7422, doi:10.1016/j.jcp.2008.04.026, 2008.

Zerroukat, M. and Allen, T.: A three-dimensional monotone and conservative semi-Lagrangian scheme (SLICE-3D) for transport problems, Q.J.R. Meteorol. Soc., 138: 1640-1651. doi: 10.1002/qj.1902, 2012
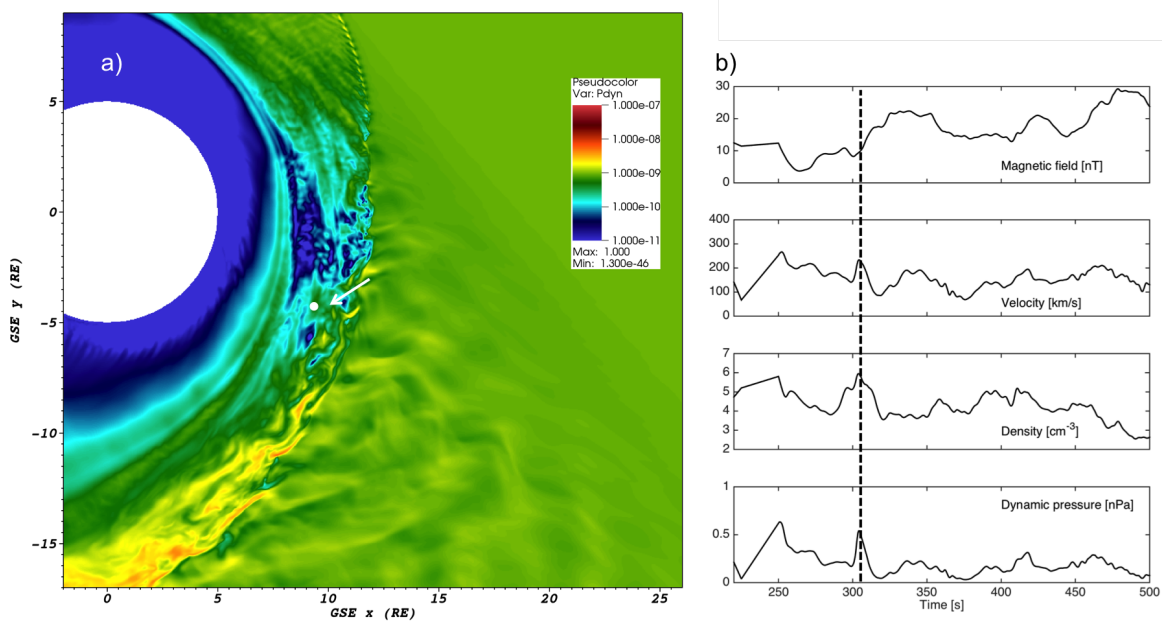
Figure 1. a) Dynamic pressure within Vlasiator simulation domain. The figure is a snapshot of Supplementary movie S1. The arrow indicates the visually detected magnetosheath jet under scrutiny in this paper. b) Virtual spacecraft data from the location marked with a white dot in panel a): Magnetic field, velocity, density and dynamic pressure as a function of time. The dashed vertical line shows the time of the visually identified jet.
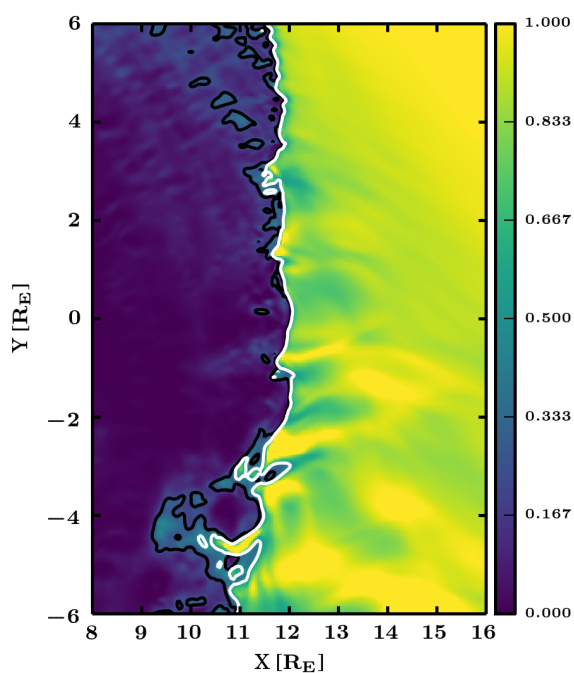
Figure 2. Colour-coding shows the dynamic pressure calculated using the X-component of velocity, v_X, divided by the solar wind dynamic pressure using the solar wind v_X. The black contour shows where this Plaschke criterion exceeds 0.25, and white where it exceeds 0.5, as defined in Plaschke et al. (2013).
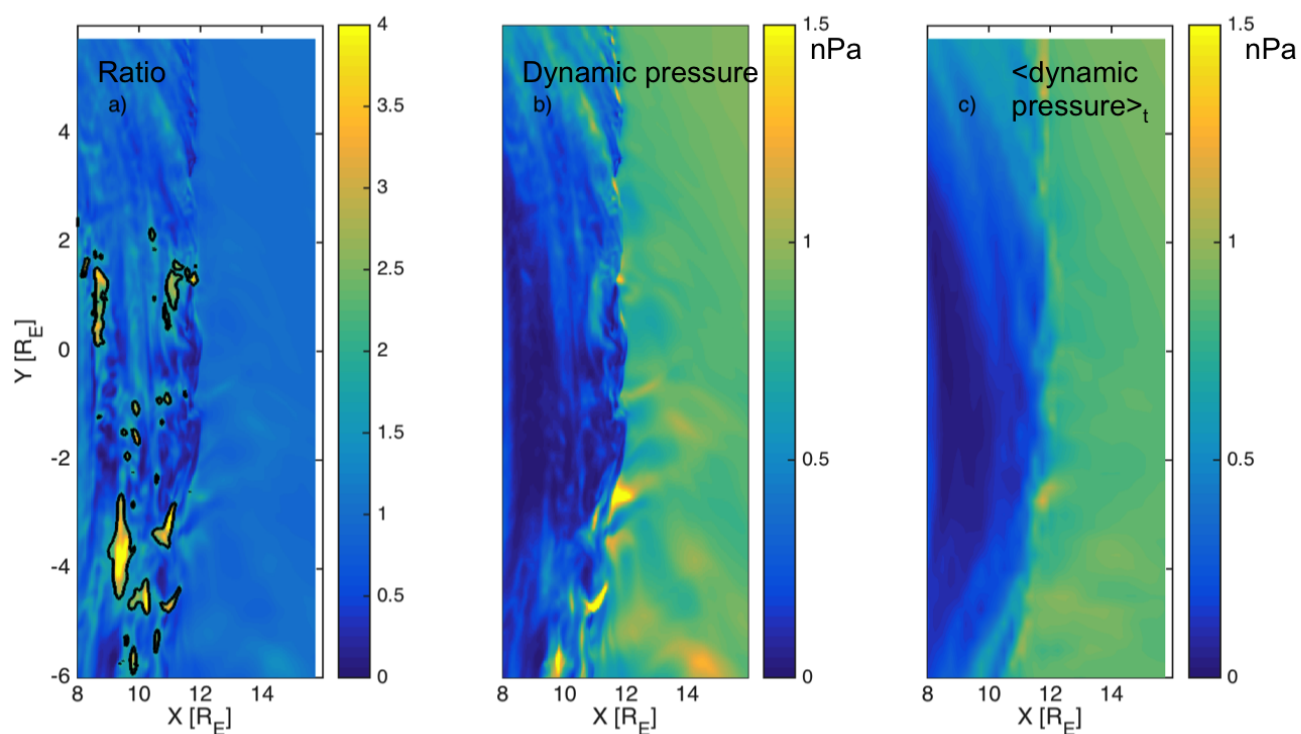
Figure 3. a) The Archer and Horbury (2013) criterion defined in Eq. (2), devised from the ratio of b) the dynamic pressure and c) the temporal average of dynamic pressure over three minutes centered at the time showing the jet-like feature in Fig. 1a. Panel a) shows a contour marking the locations where the ratio of panel b) and c) exceeds 2.
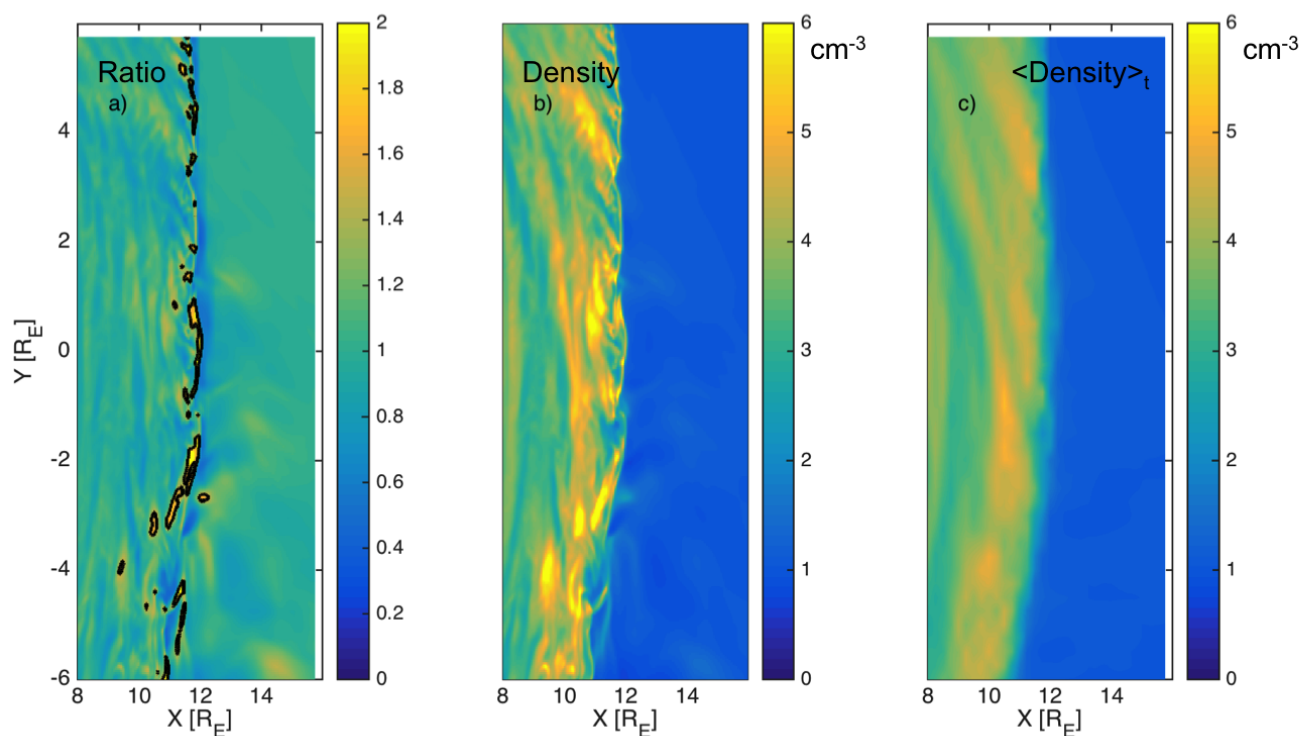
Figure 4. a) The Karlsson criterion in Eq. (3) (Karlsson et al., 2012, 2015), devised from the ratio of b) the density and the c) temporal average of density over three minutes, centered at the time showing the jet-like feature in Fig. 1a. Panel a) shows a contour marking locations where the ratio of panel b) and c) exceeds 1.5.
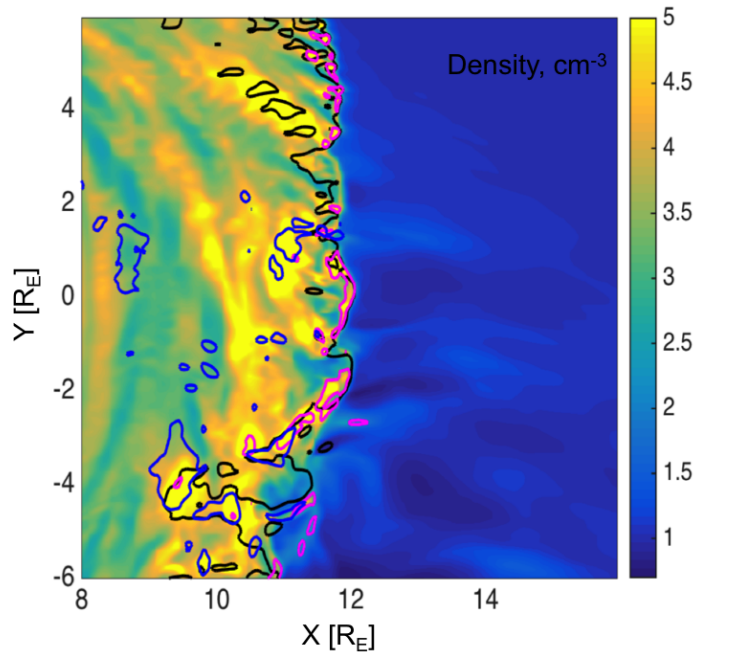
Figure 5. All criteria with density colour-coded at $t = 305.5$ s. The Karlsson criterion C_K in Eq. (3) is given with magenta, Archer and Horbury criterion C_A in Eq. (2) with blue, and the Plaschke criterion C_P in Eq. (1) with black.
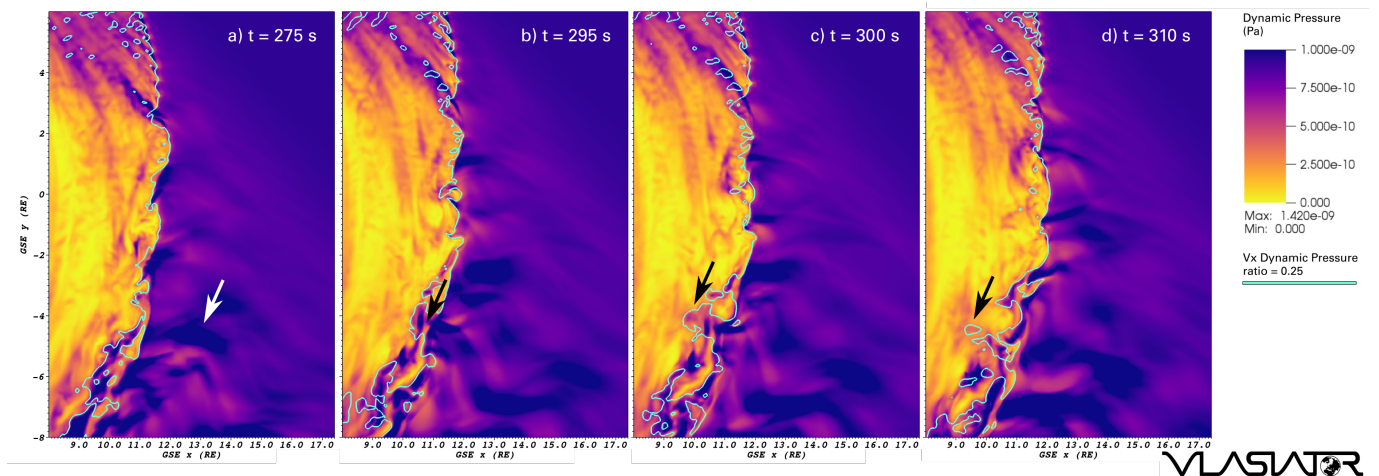
Figure 6. Time evolution of the jet. The color coding in the background shows the total dynamic pressure, while the cyan contour shows the Plaschke criterion C_P computed using the X component of the velocity v_X in dynamic pressure. Panels a) to d) show times 275, 295, 300, and 310 seconds, respectively, from the start of the simulation. The time of the jet at its prime is shown in Fig. 5. The arrows show the jet generation and are referred to in the text. The panels are snapshots of Supplementary movie S2.